

# Dual JPEG Compatibility: a Reliable and Explainable Tool for Image Forensics

Etienne Levecque, Jan Butora, Patrick Bas

**Abstract**—Given a JPEG pipeline (compression or decompression), this paper shows how to find the antecedent of a  $8 \times 8$  block. If it exists, the block is *compatible* with the pipeline. For unaltered images, all blocks are always compatible with the original pipeline; however, for manipulated images, this is not always the case. This article demonstrates the potential of compatibility concepts for JPEG image forensics. It presents a solution to the main challenge of finding a block antecedent in a high-dimensional space. This solution relies on a local search algorithm with restrictions on the search space. We show that inpainting, copy-move, or splicing applied after a JPEG compression can be turned into three different mismatch problems and be detected. In particular, when the image is re-compressed after the modification, we can detect the manipulation if the quality factor of the second compression is higher than the first one. Our method can pinpoint forgeries down to the JPEG block with great detection power and without False Positive. We compare our method with two state-of-the-art models on localizing inpainted forgeries after a simple or a double compression. We show that under our working assumptions, it outperforms those models for most experiments.

**Index Terms**—JPEG Forensics, JPEG Compatibility, Forgery localization.

## I. INTRODUCTION

Nowadays, image editing has become incredibly easy, making reliable image forensic methods more crucial than ever. Almost anyone can alter an image using licensed software or free smartphone apps, and the results are often convincing. While most modifications are benign, some can become malicious. For instance, misinformation can involve deleting, adding, or altering important data in an image. Such images containing fake information can sometimes have serious consequences, including influencing public opinion in politics, falsifying scientific findings, or triggering harassment on social networks.

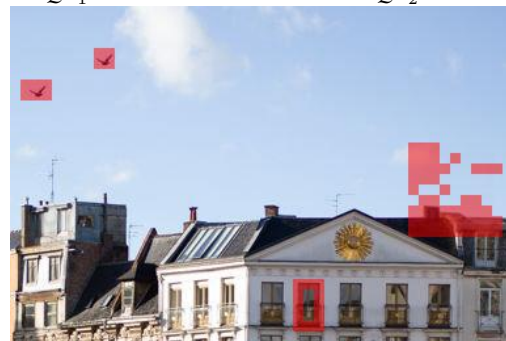
In this paper, we leverage the fact that digital images are usually compressed. This is a common practice on the Internet, where reducing data traffic is a top priority. Of all the image compression methods, the most widespread is undoubtedly JPEG compression (Joint Photographic Experts Group). It was one of the first methods to be adapted to many applications and to retain good visual rendering. This popularity has been maintained over time, and many cameras still save images in JPEG by default. However, as we will see later, many papers in the literature show that JPEG compression artifacts can be used to gather information about media authenticity.

There are many different ways of altering an image. In our case, we are focusing on images that have already undergone



(a) Original JPEG image at  $QF_1 = 80$

(b) Forged JPEG image at  $QF_2 = 85$



(c) Detection results on the decompressed JPEG.

Fig. 1: Demonstration of finding incompatible JPEG blocks. The chimney was removed using in-painting (*i.e.* uncompressed data), and birds were spliced with different Quality Factors ( $QF$ s), one of them is fully aligned with the JPEG grid but not the other. The window was copy-moved aligned on the JPEG grid but not fully aligned, *i.e.* portions of blocks belong to the original image.

JPEG compression, and were then modified in the pixel domain. The first modification is the *copy-move* which involves selecting a portion of the image, duplicating it, and pasting it elsewhere. If the portion comes from another image, this is known as *splicing*. Additionally, it is possible to locally change the pixel values to add or remove content, a process referred to as *inpainting*.

Our approach fits into this context of verifying the authenticity of JPEG images and, in particular, detecting local forgeries. The proposed method does not allow for the detection of global image forgeries or the generation of entire images. Our verification mechanism is based on the concept of block compatibility. We try to answer the following question: If we observe an  $8 \times 8$  block **B**, is there a block **A** which, once passed through the JPEG pipeline, would give **B**? If so, the block is compatible with the pipeline; if not, it is incompatible and has been altered. By construction, all unmodified images

are compatible with their development pipeline. But when modifications are made to the pixels of a decompressed image, it is often possible to create a block that is impossible to obtain through compression of a block of pixels, an incompatible block, and therefore a modified block. While the idea is simple, proving whether or not a block is compatible is a complex problem in very high dimensions. However, this approach has a significant advantage: unmodified images are inherently compatible, so there are no false positives.

Our contributions are the following:

- We propose a dual extension of the antecedent search used in steganalysis [13]. The previous method looks for a DCT (Discrete Cosine Transform) antecedent of a pixel block, whereas the proposed algorithm can fit any pipeline with any number of compressions or decompressions. This search can find antecedents in the pixel or DCT domain and can find antecedents for integer DCT pipelines.
- A phylogenetic approach of all JPEG forgery scenarios (see Section V) shows that all pixel modification can fall into three types of compatibility mismatch: the grid mismatch, the quantization mismatch, and the pipeline mismatch. Solving each type of mismatch ensures solving the vast majority of JPEG forgery.
- We analyze the impact of the Quality Factor ( $QF$ ) over the compatibility result in each mismatch case and show that for some combinations of  $QF$  the search is fast on compatible blocks. Additionally, the detection is deterministic, *i.e.* contrary to statistical methods, there are no false positives: a block detected as incompatible has been tampered with.
- Finally, we conduct experiments to show that compatibility can be used to build a JPEG forgery detector that achieves state-of-the-art performance. This method is very self-explainable, can gather information about the falsified areas, and localize forgery at the JPEG block level.

Section II presents works related to this paper, in particular about JPEG forgery detection and JPEG compatibility. The section III defines the main notations for JPEG compression, decompression, and composed pipelines. The compatibility is presented in section IV along with the algorithm to prove that a block is compatible or not. Section V formulates all JPEG forgery scenarios into 3 mismatches that can create incompatible blocks and therefore could be detected with compatibility. Finally, section VI compares our JPEG forgery detector based on incompatibility with other JPEG-oriented detectors.

## II. RELATED WORKS

### A. Forgery detection

To tackle the detection of falsified JPEG images, literature can be split into two categories: on one hand, there are the statistical methods built over an underlying constrained model: if the observed features do not follow the model, the image is classified as forged. On the other hand, there are statistical methods built with data that encompass supervised

deep learning approaches that extract complex features, often lacking explainability, to classify or segment the image into tempered or non-tempered regions.

In the first category, Lukas *et al.* [16] estimates the primary quantization table of a double compressed image with the presence of peaks in the DCT histograms. The main limitation is that it is hard to estimate the high-frequency quantization step, especially for low  $QF$ s, because nearly all or all the coefficients are quantized to 0. Farid *et al.* [7] propose a forgery detection based on a JPEG ghost. It is related to the convergence of multiple compression at the same quality factor: if a block was double compressed, compressing it at the same  $QF$  will return a very close value, but for an uncompressed block or block compressed with a different  $QF$ , the difference will be more important. This difference reveals a darker region called "ghost". This method was automated for forgery detection in Zach's *et al.* [21] paper. Performances are good except when the modified area has been compressed with a lower  $QF$  than the  $QF$  of the image. Another category of methods relies on different versions of Benford's law [9], [18], [19] applied on DCT coefficients to derive statistical tests used to detect single/double compression or estimate the different  $QF$  used in the pipeline.

In the second category, we find deep learning detectors that specifically target modified JPEG images such as the convolutional neural networks proposed by Barni *et al.* [2] to detect aligned or non-aligned double JPEG compression. Detecting double compression when the first quality factor is larger than the second one is a challenging task, but their results using the noise residuals and the pixel values are promising in this direction for non-aligned double compression. However, the generalization over multiple  $QF$ s is not achieved since they need different datasets to train multiple models. Cat-Net, the model proposed in the paper of Kwon *et al.* [12] takes these performances a step further with a good generalization over multiple forgery scenarios and  $QF$ s. This model uses DCT volume representation instead of histograms and combines it with pixel values to detect JPEG compression artifacts at a pixel level.

Also in the second category, there are deep learning models not specific to JPEG images such as ManTra-Net, the model proposed by Wu *et al.* [20]. This model targets each type of image forgeries and the JPEG compression or double compression are only two classes among many others. If their visual segmentation is very satisfying, the misclassification error between single-compressed and double-compressed is close to 85%. Another general model is Noiseprint proposed by Cozzolino *et al.* [5] which relies on camera fingerprint estimation to detect that an image has been forged. Using contrastive learning, the authors train a model to estimate the so-called "noiseprint" of an image that can generalize this operation on unseen cameras. However, the main drawback of this scheme is its dependence on the  $QF$  since they need to train a specific detector for each quantization matrix. Finally, TruFor is an improved version of Noiseprint proposed in Guillard's *et al.* paper [10] which also relies on an estimation of camera noiseprint to localize forgeries. This model aims at detecting splicing but generalizes quite well on any forgery

type when there is sufficient pattern in the fingerprint, which is the case with JPEG compression.

### B. JPEG compatibility

The compatibility notion in JPEG blocks is not recent, the first paper to present and use it is the one of Fridrich *et al.* [8]. To verify the compatibility of a block, they filter potential antecedent candidates with the  $\ell_2$ -distance from those candidates to the recompressed DCT block. They show that this distance can be upper-bounded by the norm of the worst-case scenario of rounding error. This constraint highly reduces the number of candidates for small  $QF$ s but not for  $QF$ s higher than 95. The method is very powerful but limited to grayscale images. The second limitation is that the guarantee for the compatibility is built with the mathematical Discrete Cosine Transform (DCT). Although the mathematical definition of the DCT is linear and bijective, most of the implementations do not respect those properties as detailed in section IV.

Compatibility has been extended to the reverse case (verifying the compatibility of a DCT block) in Butora's *et al.* [4] work. The authors propose a statistical model for the variance of the rounding error due to decompression. It is used to train a neural network to detect steganographic messages embedded in the DCT domain of JPEG images. A similar model was used in Dworetzky's *et al.* [6] work to detect steganographic messages embedded in the spatial domain.

The work of Lewis *et al.* [14] is not about detecting modification in JPEG images but doing exact recompression of a decompressed JPEG image. To do so, they try to find the exact DCT block of the observed pixel block, in other words, they search for an antecedent of a pixel block. The search is built with a very interesting set refining method: each step of the compressor tries to inverse a step of the decompressor by refining a set of possible values. At the end of the compression, the exact DCT antecedent should be the only one in the set. This method can deal with color images but the complexity at  $QF$ s higher than 90 makes it intractable.

An antecedent search was already used in [13] to find pixel antecedents of a DCT block. The methodology is similar but was applied to steganalysis at  $QF = 100$ . In the dual formulation formulated in the present paper (see section IV), it appears that blocks are more likely to become incompatible when the modifications are done in the pixel domain which makes the JPEG compatibility much more general and allows forgery detection for a wide range of  $QF$ s.

## III. JPEG PIPELINE

### A. Notations

We consider that an image is divided into non-overlapping blocks of size  $(c, 8, 8)$  pixels with  $c$  the number of channels (1 for grayscale, 3 for color images). The analysis of chrominance sub-sampling is beyond the scope of this study but should be addressed in a future work. We suppose for simplicity that the image size can be divided by 8. All operations in this paper are block independent, therefore we will use the same bold letter to refer to the image or to a block of this image. We use the letter  $\mathbf{Q}$  to denote the

quantization table of the same size  $(c, 8, 8)$  as the block. The standard multiplication  $x \times y$  and division  $\frac{x}{y}$  symbols are used to define element-wise operations. The dot product  $x \cdot y$  is used to refer to the matrix product. The rounding operator is defined as  $[x]$ . The notation tilde  $\tilde{\cdot}$  is used to indicate a floating-point vector.

We only present some mathematical formulation of the JPEG pipeline that will be used in the rest of the paper.

**Color transformation:** Only RGB pixels undergo color transformation to become YCbCr pixels (denoted YCC). The mathematical definition of this transformation is linear and bijective and can be applied independently for every pixel  $\mathbf{x}_{\text{RGB}} \in [0; 255]^3$  with the matrix  $\mathbf{T}$  as follows:

$$\mathbf{x}_{\text{YCC}} = \mathbf{T} \cdot \mathbf{x}_{\text{RGB}} + \begin{pmatrix} 0 \\ 128 \\ 128 \end{pmatrix}. \quad (1)$$

$$\mathbf{x}_{\text{RGB}} = \mathbf{T}^{-1} \cdot \left( \mathbf{x}_{\text{YCC}} - \begin{pmatrix} 0 \\ 128 \\ 128 \end{pmatrix} \right). \quad (2)$$

with  $\mathbf{T} \cdot \mathbf{T}^{-1} = \mathbf{I}_3$  and,

$$\mathbf{T} = \begin{pmatrix} 0.299 & 0.587 & 0.114 \\ -0.168736 & -0.331264 & 0.5 \\ 0.5 & -0.418688 & -0.081312 \end{pmatrix}. \quad (3)$$

However, most implementations of this color transformation round the result to the nearest integer and use only integer and bit shift (`libjpeg` [11] for instance) making them neither linear nor invertible. In these cases, we will use  $t$  and  $t_b$  to denote the color transformation and its backward transformation.

**JPEG compression:** The JPEG compression is applied independently on every channel of every block. Let  $\mathbf{x}$  be a pixel block. Its Discrete Cosine Transform (DCT) coefficients  $\mathbf{c}$  can be defined as follows:

$$\tilde{\mathbf{c}} = \frac{\text{DCT}(\mathbf{x})}{\mathbf{Q}}, \quad (4)$$

$$\mathbf{c} = [\tilde{\mathbf{c}}]. \quad (5)$$

where DCT refers to the forward 2D Discrete Cosine Transform function and  $\mathbf{Q}$  is the quantization table of the same size as a block, which depends on the  $QF$  of the compression. A high  $QF$  means small quantization steps (at  $QF = 100$ , the quantization steps are all equal to 1). DCT algorithm and rounding operation are not unique, there exist several types of implementation depending on the application. Therefore we use the notations  $\mathbf{c} = \mathcal{C}(\mathbf{x}; \mathbf{Q})$  to define a specific compressor.

**JPEG decompression:** The decompression process is almost symmetrical. Given a DCT block  $\mathbf{c}$ , the decompressed pixel block is:

$$\tilde{\mathbf{y}} = \text{IDCT}(\mathbf{Q} \times \mathbf{c}), \quad (6)$$

$$\mathbf{y} = [\tilde{\mathbf{y}}]^{[0; 255]}, \quad (7)$$

where the notation  $[\cdot]^{[0;255]}$  means that the results of the rounding operation are clipped to the set  $[0;255]$ . For the same reason as for the compressor, we use the notation  $\mathbf{y} = \mathcal{D}(\mathbf{c}; \mathbf{Q})$  to define a specific implementation of a decompressor.

As said for the compressor and decompressor, there exist several implementations of the DCT and IDCT algorithms to find a good trade-off between speed and precision for each application [1], [15]. The same applies to the color transformation. In this paper, we focus on the default algorithm from `libjpeg` library [11] called `islow`. We also did all our experiments with the `libjpeg` color transformation that uses integers and thus is not lossless.

### B. Composed Pipelines

To deal with double compression or more means that compression and decompression must be composed multiple times with potentially different functions and parameters. We define those notations in this subsection.

Let  $f_1, \dots, f_n$  be  $n > 0$  compression or decompression functions alternated. This means that for each consecutive pair  $(f_i, f_{i+1})$  there is a compression and a decompression. If  $n = 1$ , the pipeline is only composed of a single function that can be either a compression or a decompression. Each function is parameterized by its quantization tables  $\mathcal{Q} = (\mathbf{Q}_1, \dots, \mathbf{Q}_n)$ . We denote the composed pipeline as  $\mathcal{F}(\cdot; \mathcal{Q})$ .

For example, if we have  $f_1$  a decompression with quantization matrix  $\mathbf{Q}_1$  and  $f_2$  a compression function with the quantization matrix  $\mathbf{Q}_2$ , then the composed pipeline of  $f_1$  and  $f_2$  is  $\mathcal{F}$  parameterized with  $\mathcal{Q} = (\mathbf{Q}_1, \mathbf{Q}_2)$  and for any block  $\mathbf{x}$ ,

$$\mathcal{F}(\mathbf{x}; \mathcal{Q}) = f_2(f_1(\mathbf{x}; \mathbf{Q}_1); \mathbf{Q}_2). \quad (8)$$

We also define the backward pipeline as  $f_b$  ( $\mathcal{F}_b$  for composed pipelines) that takes as argument a block from the same domain as  $\mathbf{y}$  and return a block in the same domain as  $\mathbf{x}$ . For example if  $\mathcal{F}$  is a decompression at  $\mathbf{Q}_1$  followed by a compression at  $\mathbf{Q}_2$ ,  $\mathcal{F}_b$  is a compression at  $\mathbf{Q}_2$  followed by a decompression at  $\mathbf{Q}_1$ .

Regardless of implementations used in the forward pipeline  $\mathcal{F}$ , the backward pipeline  $\mathcal{F}_b$  can be defined with any DCT, IDCT, or color transformation algorithms. Therefore, we always define it with the floating-point bijective algorithms to avoid any error due to integer operation. Moreover, we do not round or clip any result in this backward pipeline, making it perfectly reversible.

However, note that due to rounding operations,  $f$  is not an invertible function, and thus  $f$  and  $f_b$  are not inverse functions of each other:  $f(f_b(\mathbf{y}; \mathbf{Q}); \mathbf{Q}) \neq \mathbf{y}$  ( $\mathbf{y}$  is an arbitrary block in the domain of  $f_b$ ) and  $f_b(f(\mathbf{x}; \mathbf{Q}); \mathbf{Q}) \neq \mathbf{x}$  most of the time. The same applies to  $\mathcal{F}$  and  $\mathcal{F}_b$ .

## IV. JPEG COMPATIBILITY

### A. Definitions and challenges

In this subsection, we define JPEG compatibility as the existence of a solution to an inverse problem.

Let  $\mathbb{S}$  be the set of pixel blocks or the set of DCT blocks. Let  $\mathbf{y} \in \mathbb{S}$  be a block and let  $f$  be a function of compression or decompression such that the codomain (set of destination) of  $f$  is  $\mathbb{S}$ . Let  $\mathbf{Q}$  be the quantization table that parameterizes  $f$ . We say that  $\mathbf{y}$  is *compatible* with  $f$  if there exists a block antecedent  $\mathbf{x}$  such that:

$$f(\mathbf{x}; \mathbf{Q}) = \mathbf{y}. \quad (9)$$

On the contrary, if no antecedent  $\mathbf{x}$  exists, we say that  $\mathbf{y}$  is *incompatible* with  $f$ .

We can easily generalize this definition to any composed pipeline  $\mathcal{F}$  with the set of quantization tables  $\mathcal{Q}$  and codomain  $\mathbb{S}$ :

$$\mathcal{F}(\mathbf{x}; \mathcal{Q}) = \mathbf{y}. \quad (10)$$

This inverse problem is complex because the pipeline is not an invertible function and thus applying the backward pipeline to  $\mathbf{y}$  will return a close candidate but not always an antecedent. Even if we suppose that the uniform norm between this close candidate and the closest antecedent is 1, this means that for each element in the blocks, the error can be one of -1, 0, or 1. This sums to  $3^{64}$  possibilities for grayscale blocks and  $3^{192}$  possibilities for color blocks without colors sub-sampling. Brute forcing all solutions can not be considered, instead, we will rely on a local search to find antecedents combined with theoretical constraints to reduce the search space.

### B. Local search to find antecedents

The local search is detailed in algorithm 1 and shares some similarities with the one presented in [13]. However, this one can be used with any composed or simple pipeline and uses the  $\ell_1$  norm instead of the infinity norm.

---

#### Algorithm 1 Local search to find antecedent

---

**Require:**  $\mathbf{y}, \mathcal{Q}$  {Observed block and quantization tables}  
**Require:**  $\mathcal{F}$  {Pipeline}  
**Require:**  $N > 0$  {Max iteration}  
 $\mathbf{x}_s \leftarrow \mathcal{F}_b(\mathbf{y})$  {Starting block of the search}  
add  $\mathbf{x}_s$  to  $P$  with cost 0 {Priority queue initialization}  
**while**  $P$  not empty **and**  $k \leq N$  **do**  
 $k \leftarrow k + 1$   
 $\mathbf{x} \leftarrow$  remove first element of  $P$   
**for**  $\mathbf{x}_n$  in  $neighbors(\mathbf{x})$  **do**  
**if**  $\mathbf{x}_n$  has not been visited **then**  
**if**  $\mathcal{F}(\mathbf{x}_n; \mathcal{Q}) = \mathbf{y}$  **then**  
**return**  $\mathbf{x}_n$  { $\mathbf{x}_n$  is an antecedent of  $\mathbf{y}$ }  
**end if**  
 $c_n \leftarrow \|\mathbf{y} - \mathcal{F}(\mathbf{x}_n; \mathcal{Q})\|_1$   
add  $\mathbf{x}_n$  to  $P$  with cost  $c_n$  { $\mathbf{x}_n$  is a new candidate}  
**end if**  
**end for**  
**end while**

---

The search begins by applying the backward pipeline to the observed block to obtain a starting candidate. Then, until the number of iterations is reached, we select the best candidate from a priority queue (queue data structure but every element

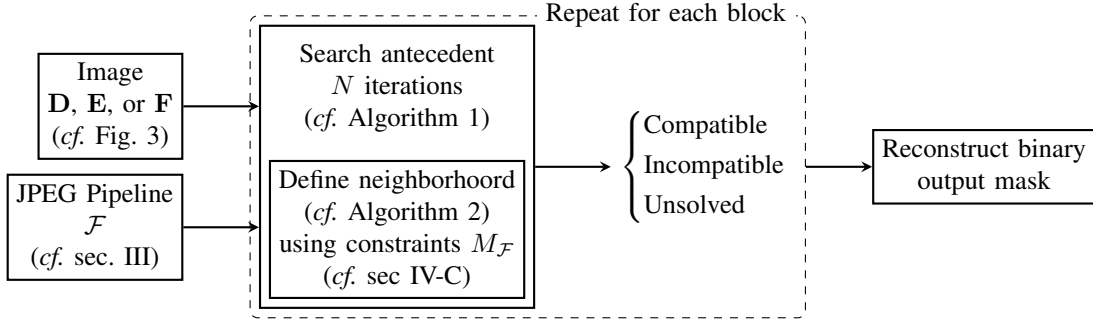


Fig. 2: General flowchart of our method. For each block of the image obtained with a pipeline  $\mathcal{F}$ , we search an antecedent with a local search constrained with upper bound  $M_{\mathcal{F}}$ . If the block is incompatible, we can conclude that it was altered. If the block is unsolved, the decision is left to the agent depending on the number of iterations  $N$ .

has a priority; highest priority is always first), explore all its neighbors, and feed the priority queue again depending on the  $\ell_1$  distance to the observation. If the distance is 0, then an antecedent has been found and the search returns the result. A hash table is used to ensure that each block is visited only once.

The neighborhood of a candidate is defined in Algorithm 2 with  $M_{\mathcal{F}}$  an upper bound depending on the pipeline  $\mathcal{F}$  that will be defined in the next subsection. However, when the block  $\mathbf{x}$  is clipped, we ignore this upper bound and always add the new candidate to the neighborhood. Note that we only apply changes of  $\pm 1$  to one single value in the block but this process is repeated indefinitely until the maximum number of iterations is reached. Hence, every block in the constrained search space can be explored.

---

#### Algorithm 2 Neighbors function

---

**Require:**  $\mathbf{x}$  {Block for which a neighborhood is required}

**Require:**  $\tilde{\mathbf{x}}_b$  {Floating point starting point}

**Require:**  $M_{\mathcal{F}}$  {Upper bound of the pipeline}

```

for  $i$  in channels do
  for  $j$  in rows do
    for  $k$  in columns do
       $\mathbf{x}_n \leftarrow \text{copy}(\mathbf{x})$ 
       $x_{n,i,j,k} \leftarrow x_{n,i,j,k} + 1$  {Positive change}
      if  $\|\mathbf{x}_n - \tilde{\mathbf{x}}_b\|_2 \leq M_{\mathcal{F}}$  then
        add  $\mathbf{x}_n$  to the neighborhood
      end if
       $\mathbf{x}_n \leftarrow \text{copy}(\mathbf{x})$ 
       $x_{n,i,j,k} \leftarrow x_{n,i,j,k} - 1$  {Negative change}
      if  $\|\mathbf{x}_n - \tilde{\mathbf{x}}_b\|_2 \leq M_{\mathcal{F}}$  then
        add  $\mathbf{x}_n$  to the neighborhood
      end if
    end for
  end for
end for
return neighborhood
  
```

---

Note that to find an antecedent, this local search algorithm can be considered as fast. Indeed, the worst case is for  $QF = 100$  because lots of candidates are very close to the solution and can be solved in a matter of minutes for most blocks.

However, the problem is for incompatible blocks, the search could explore the whole intractable space before emptying the priority queue. We can avoid that by constraining the searching space and thus the neighborhood.

#### C. Additional theoretical constraints

In order to speed up the search of incompatible blocks we also decided to see to which extent we can use the criterion proposed in the paper of Fridrich *et al.* [8] where the authors defined a theoretical constraint for grayscale candidate blocks that drastically reduce the search space for  $QF < 95$ . This constraint is presented in this subsection as well as the generalization to color images and double compression. All computations are done under two assumptions. First, we are using the mathematical definition of the DCT, the IDCT, and the color transformation such that all of them are unitary invertible functions. Second, we suppose that there is no clipping in the sense that all pixel values are always in the interval  $[0;255]$ . This second assumption is necessary otherwise, the rounding error can be bigger than  $1/2$  and the constraints will not hold.

Let's start with intermediate results that will simplify the equations. Let  $\tilde{\mathbf{y}}$  be a floating point block of size  $8 \times 8$  and  $\mathbf{y} = [\tilde{\mathbf{y}}]$  its rounding value. We define the rounding error as  $\mathbf{e} = \mathbf{y} - \tilde{\mathbf{y}}$ . We have the following upper bound on the rounding error norm:

$$\begin{aligned}
 \|\mathbf{y} - \tilde{\mathbf{y}}\|_2 &= \sqrt{\sum_{i=1}^8 \sum_{j=1}^8 |y_{i,j} - \tilde{y}_{i,j}|^2} \\
 &\leq \sqrt{\sum_{i=1}^8 \sum_{j=1}^8 \frac{1}{2}} \\
 &\leq 4.
 \end{aligned} \tag{11}$$

Now if we have a color transformation, we use the under-script  $RGB$  to denote the  $3 \times 8 \times 8$  tensor with the three channels, and  $Y$ ,  $R$ ,  $G$ , and  $B$  for each individual channel. The same result applies to other channels:

$$(T \cdot \mathbf{e}_{RGB})_Y = 0.299\mathbf{e}_R + 0.587\mathbf{e}_G + 0.114\mathbf{e}_B. \tag{12}$$

Since each row of  $T$  sums to one, we can invoke the triangle inequality together with equation (11) to upper bound each channel by 4 and obtain:

$$\|T \cdot ((\tilde{\mathbf{y}}_{RGB}) - \mathbf{y}_{RGB})_Y\|_2 \leq 4. \quad (13)$$

Note that we have the same upper bound when doing the inverse color transform.

We now derive two upper bounds, one that is used when searching for an antecedent of a compression, and one used when searching antecedent of a decompression.

Let us consider a simple compression setup with notations  $\mathbf{x}$ ,  $\mathbf{Q}$ ,  $\tilde{\mathbf{c}}$  and  $\mathbf{c}$  defined in equations (5), (4). This compression can be modeled by a pipeline  $f$  and its backward equivalent  $f_b$ . We suppose that we observe  $\mathbf{c}$  and would like to find the antecedent  $\mathbf{x}$  from the starting point  $\mathbf{x}_b = f_b(\mathbf{c})$ . To speed up the search we will derive an upper bound to the distance between the true antecedent and the starting point:

$$\begin{aligned} \|\mathbf{x} - \mathbf{x}_b\|_2 &= \|\mathbf{x} - \text{IDCT}(\mathbf{Q} \times \mathbf{c})\|_2 \\ &= \|\mathbf{x} - \text{IDCT}(\mathbf{Q} \times \mathbf{c} - \mathbf{Q} \times \tilde{\mathbf{c}} + \mathbf{Q} \times \tilde{\mathbf{c}})\|_2 \\ &= \|\mathbf{x} - \mathbf{x} - \text{IDCT}(\mathbf{Q} \times \mathbf{c} - \mathbf{Q} \times \tilde{\mathbf{c}})\|_2 \\ &= \|\mathbf{Q}(\mathbf{c} - \tilde{\mathbf{c}})\|_2 \\ &\leq M_f = \left\| \frac{\mathbf{Q}}{2} \right\|_2 \end{aligned} \quad (14)$$

Indeed, the  $\ell_2$ -norm is invariant by unitary transformation (the IDCT) and the inequality comes from (11) with a quantization table.

Now, let's consider a decompression setup with notations  $\mathbf{Q}$ ,  $\mathbf{c}$ ,  $\tilde{\mathbf{y}}$  and  $\mathbf{y}$  defined in equations (5), (6) and (7). This decompression can also be modeled by a pipeline  $f$  and its backward equivalent  $f_b$ . We suppose that we observe  $\mathbf{y}$  and would like to find the antecedent  $\mathbf{c}$  from the starting point  $\mathbf{c}_b = f_b(\mathbf{y})$ . Using a very similar calculus, we derive an upper bound to the distance between the true antecedent and the starting point:

$$\begin{aligned} \|\mathbf{Q}\mathbf{c} - \mathbf{Q}\mathbf{c}_b\|_2 &= \|\mathbf{Q}\mathbf{c} - \text{DCT}(\mathbf{y})\|_2 \\ &= \|\mathbf{Q}\mathbf{c} - \text{DCT}(\mathbf{y} - \tilde{\mathbf{y}} + \tilde{\mathbf{y}})\|_2 \\ &= \|\mathbf{Q}\mathbf{c} - \mathbf{Q}\mathbf{c} - \text{DCT}(\mathbf{y} - \tilde{\mathbf{y}})\|_2 \\ &= \|\mathbf{y} - \tilde{\mathbf{y}}\|_2 \\ &\leq M_f = 4. \end{aligned} \quad (15)$$

Using the triangle inequality of the norm, this constraint can be generalized to any pipeline by adding the upper bounds together. For example, if we want to search for an antecedent through a pipeline of decompression (upper bound is 4) with color transform (upper bound is also 4), the distance between the starting point and the true antecedent should not exceed  $M_{\mathcal{F}} = 4 + 4$ . In the double compression scenario, the pipeline is composed of a decompression ( $M_f = 4$ ), a color transform ( $M_f = 4$ ), a compression with quantization table  $\mathbf{Q}$  ( $M_f = \|\mathbf{Q}/2\|_2$ ), another decompression ( $M_f = 4$ ) and a final color transform ( $M_f = 4$ ), then the distance should not exceed  $M_{\mathcal{F}} = 4 + 4 + \|\mathbf{Q}/2\|_2 + 4 + 4$ .

Finally, each upper bound obtained defines a sphere around the starting point in which the true antecedent should be. If

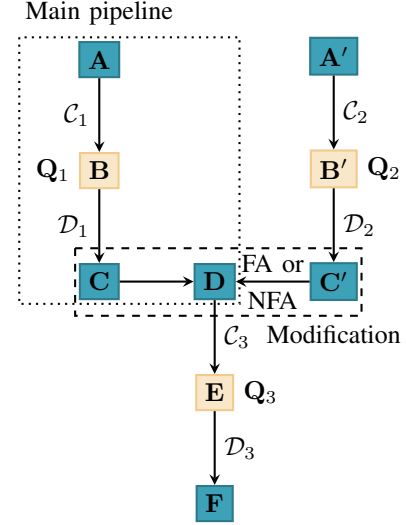


Fig. 3: General scenario for modifying a JPEG image in the spatial domain. Blues boxes represent blocks in the spatial domain (pixels) and orange boxes represent blocks in the frequency domain (DCT coefficients).  $\mathcal{C}$  and  $\mathcal{D}$  are the compressors and decompressors used.  $\mathbf{Q}$  are the quantization tables. Modifications applied to  $\mathcal{C}$  can be fully aligned (FA) or not fully aligned (NFA).

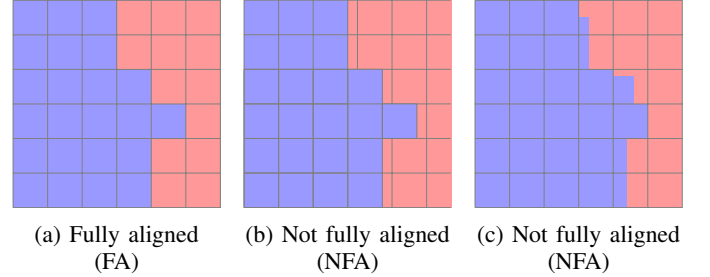


Fig. 4: Examples of fully aligned and not fully aligned modifications. Example 4b illustrates block translations from one image to another, on the contrary example 4c illustrates a finer segmentation.

we explore all candidates inside this sphere and do not find a solution to our inverse problem (9), then we can conclude that the "true antecedent" does not respect this property and the block is incompatible.

## V. COMPATIBILITY OF FORGED JPEGS

We describe in this section the different types of forgery scenarios, their associated incompatibilities, and the results associated with each scenario.

### A. Addressed forensics scenarios

There are several ways of forging a JPEG image and this section presents the underlying assumptions regarding the possible JPEG compression operations and the different scenarios that follow.

In order to verify the JPEG compatibility of an image, we need at least a part of it to come from a decompressed JPEG

image. We assume that there exists a pixel image  $\mathbf{A}$ , that has been compressed with a compressor  $\mathcal{C}_1$  and quantization table  $\mathbf{Q}_1$  to obtain the DCT coefficients  $\mathbf{B}$ . Once decompressed with a decompressor  $\mathcal{D}_1$  using the same quantization table  $\mathbf{Q}_1$ , we obtain  $\mathbf{C}$ . This pixel image  $\mathbf{C}$  is the one that will be falsified.

The general scenario, which includes all the others, is illustrated in Fig. 3. In this graph, the double arrows towards  $\mathbf{D}$  mean that the image  $\mathbf{D}$  is built by using the values of the pixels from  $\mathbf{C}$  or  $\mathbf{C}'$  and placing them at any position in  $\mathbf{D}$ . The other common part of each scenario relies on a second compression which can be applied on  $\mathbf{D}$ .

Note that the notion of fully aligned or not fully aligned altering is inspired by the definitions of aligned and non-aligned recompression formalized by Bianci and Piva [3], and is illustrated in Fig. 4. A modification is *fully aligned* (FA) if the JPEG grid of  $\mathbf{C}$  and the JPEG grid of  $\mathbf{C}'$  are the same and if all modifications are done block-wise. For example, if a block of  $\mathbf{D}$  has some pixel values from  $\mathbf{C}$  and some other pixel values from  $\mathbf{C}'$ , then the modification is not full and therefore *not fully aligned* (NFA) (*cf.* Fig. 4c). Note that the fully aligned situation is very rare when doing JPEG forgery. Indeed, if the grids can be aligned with a probability of  $\frac{1}{64}$ , blocks that form the boundary of the modification will most likely be cut, especially if a blur filter is applied to hide the contour artifacts.

Three specific forensics scenarios are described as follows, each encompassing fully aligned or not fully aligned modifications.

**Inpainting.** In this scenario, the modified pixel comes from a natural image  $\mathbf{C}'$  that has not been compressed. Therefore,  $\mathcal{C}_2$  and  $\mathcal{D}_2$  do not exist and the modifications are necessarily non-aligned since  $\mathbf{C}'$  is not associated with a JPEG grid.

**Copy-Move.** In this scenario,  $\mathbf{A} = \mathbf{A}'$ ,  $\mathbf{B} = \mathbf{B}'$  and  $\mathbf{C} = \mathbf{C}'$  (compressors and decompressors are also equal) but the image  $\mathbf{D}$  is built by taking some pixels from  $\mathbf{C}'$  and placing them somewhere else. The modifications can be aligned on the JPEG grid or non-aligned.

**Splicing.** This is the most general scenario. Two images are compressed with potentially different compressors with some quantization tables  $\mathbf{Q}_1$  and  $\mathbf{Q}_2$  that can be equal or different. The decompressed versions of those images are used to build  $\mathbf{D}$ . The modifications can be aligned on the JPEG grid or non-aligned.

### B. Possible sources of incompatibility

This subsection translates the forgery scenarios described in the previous one into three distinct mismatches that can create incompatible blocks. We denote them as the *grid* mismatch, the *quantization table* mismatch, and the *pipeline* mismatch.

**Grid mismatch** appears when the dependency between the 64 values of a block (decompressed pixels or DCT coefficients) is broken. It can be broken either because the block was partially modified and therefore there is no dependency between the two parts of the block (NFA copy-move or NFA splicing) or because the modified pixels are simply not JPEG decompressed and thus not dependent (inpainting).

**Quantization table mismatch** can only be observed when the forgery is fully aligned and when the quantization table

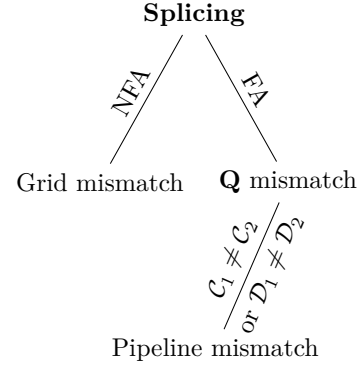


Fig. 5: In the splicing scenario, if the modifications are not fully aligned (NFA), it is a *grid* mismatch, in the fully aligned case (FA), there can be a *quantization table* mismatch if tables are not the same. *Pipeline* mismatch can appear if one of the compression or decompression (or both) differs. Note that a FA splicing with the same quantization tables and functions is a *perfect* splicing in the sense that it does not create any mismatch.

used is not the same as the one used in the main pipeline. In this case, the 64 decompressed pixel values are dependent and are not consistent with the original pipeline. This mismatch can for example be obtained when doing fully aligned splicing.

**Pipeline mismatch** can also only be observed when doing fully aligned splicing. It comes from the fact that the functions used in the compression and decompression process can be different. For example, if the DCT transform does not have the same implementation or when the rounding function is not the same. It comes from any implementation difference that influences the actual result. In particular, Fig. 5 illustrates the possible mismatches for the splicing scenario and shows that one can observe a single pipeline mismatch if compressors are not the same but decompressors are the same, or a double pipeline mismatch if both compressors and decompressors are different.

In our forgery scenario, the agent performing the analysis can observe either  $\mathbf{D}$ ,  $\mathbf{E}$ , or  $\mathbf{F}$ , so we need to explicit the type of antecedent search that needs to be carried out for each mismatch case and each observation.

Table I sums up each possible search depending on the observation and the type of mismatch. For example, if we observe a block  $\mathbf{E}$  in the DCT domain and if we want to verify that it does not suffer from grid mismatch, we need to search for a DCT antecedent such that after applying decompressor  $\mathcal{D}_1$  and compressor  $\mathcal{C}_3$  we obtain  $\mathbf{E}$ . If we can find such an antecedent, the block  $\mathbf{E}$  is compatible and there is no evidence of grid mismatch. Since the quantization mismatch relies on the same experiment, it would also give no evidence of a quantization mismatch.

### C. Statistics of incompatible blocks

In the previous section, three possible mismatches and three observations yielded nine different experiments. This



Type of mismatch	Observation		
	D	E	F
Grid	1. (DCT) $\xrightarrow{\mathcal{D}_1}$ D	2. (DCT) $\xrightarrow{\mathcal{D}_1 \mathcal{C}_3}$ E	3. (DCT) $\xrightarrow{\mathcal{D}_1 \mathcal{C}_3 \mathcal{D}_3}$ F
Quantization	4. (DCT) $\xrightarrow{\mathcal{D}_1}$ D	5. (DCT) $\xrightarrow{\mathcal{D}_1 \mathcal{C}_3}$ E	6. (DCT) $\xrightarrow{\mathcal{D}_1 \mathcal{C}_3 \mathcal{D}_3}$ F
Pipeline	7. (Pixel) $\xrightarrow{\mathcal{C}_1 \mathcal{D}_1}$ D	8. (Pixel) $\xrightarrow{\mathcal{C}_1 \mathcal{D}_1 \mathcal{C}_3}$ E	9. (Pixel) $\xrightarrow{\mathcal{C}_1 \mathcal{D}_1 \mathcal{C}_3 \mathcal{D}_3}$ F

TABLE I: This table shows the type of search depending on the type of mismatch and the observation. For example, if we observe **F** and want to verify a quantization mismatch, we are in the second row, last column, and want to find a DCT antecedent of a pipeline composed of a decompression  $\mathcal{D}_1$ , a compression  $\mathcal{C}_3$  and a second decompression  $\mathcal{D}_3$ .

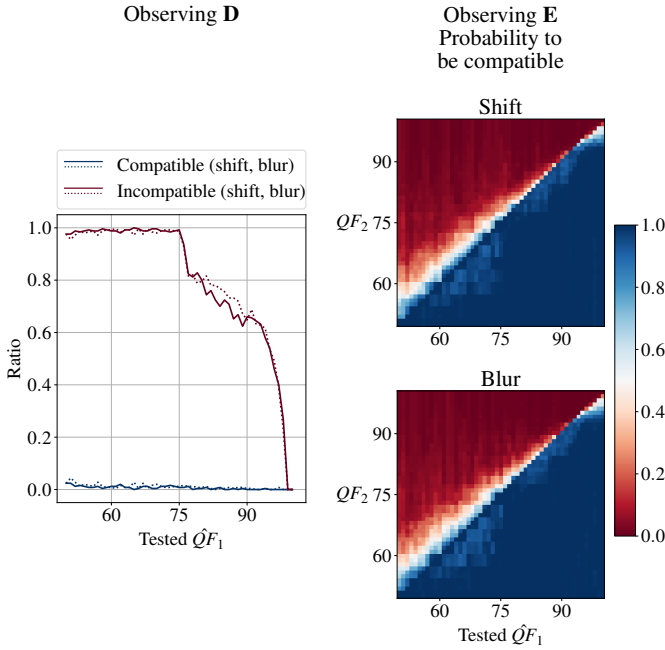


Fig. 6: Statistics in the presence of a grid mismatch due to a grid shift or a blurring kernel to remove the grid. The left plot gives ratio of compatible (blue) and incompatible (red) blocks when observing **D** and the right plots when observing **E** (almost equal to plots when observing **F**). Tested  $\hat{Q}F_1$  is the  $QF$  used to search an antecedent. Note that, all blocks have been modified in this experiment.

section presents some experiments to explore the statistics of incompatible blocks and their relation to the  $QF$ . We used images from the UCID dataset composed of 1338 RGB color images of size  $384 \times 512$ . These pixel images are equivalent to **A** in our general scenario (Fig. 3). We use the `islow` DCT method from the `libjpeg` library using all  $QF$  between 50 and 100 to create the compressed image **B**. To obtain the decompressed pixel image **C** we use the decompressor of the same library. In this subsection,  $QF_1$  and  $QF_2$  refer to the true quality factors of a block and we also use them to denote the quantization table associated with this  $QF$ . However, the tested  $\hat{Q}F_1$  refers to the  $QF$  used in the pipeline of the search.

**Statistics on grid mismatch:** We have seen in the last subsection that grid mismatch can be caused by a grid shift

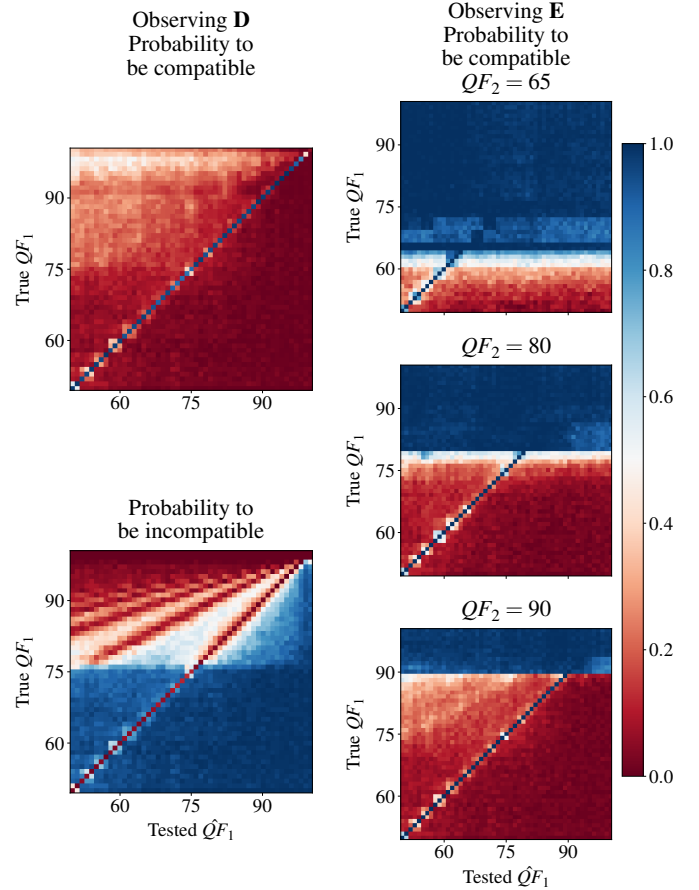


Fig. 7: Statistics in the presence of a quantization mismatch. Left plots give statistics when observing **D** and right plots when observing **E** (almost equal to plots when observing **F**). Tested  $\hat{Q}F_1$  is the  $QF$  used to search an antecedent.

(such as non-aligned splicing or copy-move) or by inpainting a region without a grid at all. To explore both cases, we try to find antecedents to blocks modified with a random misalignment (called shift) and blocks modified with a blurring kernel (called blur). We can draw the following conclusions by looking at the results in Fig. 6:

- When observing **D** (*i.e.* forged blocks in the pixel domain), blocks with a grid mismatch are very unlikely to be compatible with any tested  $\hat{Q}F_1$  (probability of being compatible almost equals to 0). For small enough tested  $\hat{Q}F_1$  we can even prove that blocks are incompatible (probability of being incompatible almost equals to 1). The search space becomes bigger with  $\hat{Q}F_1$ , so it requires more iterations in the search Algorithm 1 to explore all possible candidates. For this experiment the number of iterations was fixed to 100.
- When observing **E** (*i.e.* recompressed forged blocks), blocks with a grid mismatch are very unlikely to be compatible for tested  $\hat{Q}F_1$  small enough compared to  $QF_2$  (above diagonal tested  $\hat{Q}F_1 = QF_2$ ).
- But when observing **E**, if the tested  $\hat{Q}F_1$  is too big compared to  $QF_2$ , blocks with a grid mismatch are very likely to be compatible to this tested  $\hat{Q}F_1$  (below diagonal



tested  $\hat{QF}_1 = QF_2$ ).

- Observing **E** or **F** gives very close results.
- Shift and blur yield the same probability, so an inpainted block has the same probability of being incompatible as a non-fully aligned spliced or copy-move block.

**Statistics on quantization mismatch:** This time, observed blocks are compatible to a true  $QF_1$  but we want to evaluate how likely they are to be compatible to another tested  $\hat{QF}_1$ . Fig. 7 depicts the results of our experiments and again we can draw the following conclusions:

- When observing **D**, blocks with a quantization mismatch are very unlikely to be compatible with any other tested  $\hat{QF}_1$  different than the true  $QF_1$ . For small enough true  $QF_1$  we can even prove that blocks are incompatible with any other pipeline using a different  $\hat{QF}_1$ . We observe the same separation as for simple compression around true  $QF_1 = 75$ , which is due to the size of the search space compared to the maximum number of iterations in the search Algorithm 1.
- When observing **E**, blocks with a quantization mismatch are very unlikely to be compatible with any other tested  $\hat{QF}_1$  different than the true  $QF_1$  if  $QF_1$  is small enough compared to  $QF_2$  (below the line true  $QF_1 = QF_2$ ).
- However, when observing **E**, if  $QF_1$  is bigger than  $QF_2$ , blocks with a quantization mismatch are very likely to be compatible with any tested  $\hat{QF}_1$  (above the line true  $QF_1 = QF_2$ ).
- Observing **E** or **F** gives very close results.

**Pipeline mismatch:** This case will not be studied in this paper for two reasons. First, pipeline mismatch is very unlikely to be observed in real forged images. Second, it requires a more extensive works on studying the different DCT algorithms. We plan to study this problem in our future work.

To sum up the statistics in this subsection, if we observe the image **D** which has been modified without recompression, there is a very high chance that modified blocks due to inpainting, splicing, or copy-move will be incompatible and detected as such (we assume that fully-aligned copy-move or fully-aligned splicing with the same quantization table are rare events). And if we observe **E** (or **F**, the results should be almost the same) which have been recompressed with  $QF_2$ , we should be able to detect modified blocks due to inpainting, splicing or copy-move if  $QF_1$  is smaller than  $QF_2$ . Otherwise, we will not be able to detect anything.

## VI. FORGERY LOCALIZATION

### A. Experimental setup

One of our working assumptions is that we know each compressor and decompressor in the pipeline of our forged JPEG images. Therefore, we cannot perform the experiments on public datasets because the JPEG compression pipeline has not been entered or is simply unknown since the compression was done with the camera constructor algorithm. This set of experiments represents a proof of concept and we let the exploration of other pipelines to future works.

We consequently construct our dataset of 20 images of size  $256 \times 256$  with the `libjpeg islow` DCT algorithm using a

standard quantization table at quality factor 60, 75, or 90. After the compression, each image is decompressed with the `islow` IDCT. The decompressed pixel images are then modified using the object removal tool of Photoshop-2024 by hand.

With these forged images we can do two experiments: one without second compression and one with second compression. In the case of second compression, we again apply the `islow` DCT algorithm with standard quantization tables of 50, 60, 75, 90, and 95 to have at least a second compression with a higher  $QF$  and with a smaller  $QF$  than the first compression.

Our method can run with only 100 iterations when  $QF_1 \leq 95$  and  $QF_2 \leq 95$  and when blocks are not clipped. It's important not to ignore clipped blocks because doing so could affect the prediction, especially if there are many of them. Instead, we opted to increase the number of iterations to ensure that an antecedent is found for compatible clipped blocks. For the single compression experiment we used  $N = 100$  but for the double compression experiment, we used  $N = 5000$  iterations. We always consider unsolved blocks as incompatible to compute the metrics.

To compare our method, we use the TruFor model [10], the ZERO [17] algorithm, and the Cat-Net v2 model [12]. TruFor and Cat-Net v2 are deep neural networks trained mainly on splicing and/or copy-move datasets, however, they are both based on artifact fingerprints and the JPEG compression applied before the modification should be sufficient to have two different areas in the image: one with the JPEG artifacts and one without. Moreover, Cat-Net v2 is specifically trained to detect JPEG artifacts using an RGB stream combined with a DCT stream. These two models output a probability map, so to obtain a binary map we use a threshold of 0.5 as proposed in Cat-Net v2 paper [12].

The ZERO algorithm uses the number of zeros in the DCT representation of each block to find the JPEG grid in the image. For the inpainted region, the algorithm should not detect any JPEG grid and thus be able to localize the forgery. However, the images are rather small compared to the ones in the original paper, and forgery detection results were not satisfying even if the map of votes shows clearly that some regions of the forged image do not have any grid. Hence, we decided to show the output of the map of votes instead of the binary detection mask, and for the same reason, we cannot compute any localization metric.

The metrics used are all permuted metrics, this means that we take the best metric using the prediction or 1 minus the

	Pixel-wise				Block-wise			
	Acc	F1	AUC	FPr	Acc	F1	AUC	FPr
TruFor	78.02	61.44	92.90	4.41	79.89	65.19	91.92	5.06
Cat-Net v2	91.34	85.94	<b>99.2</b>	<b>1.61</b>	92.5	88.55	99.04	1.6
Ours	<b>98.6</b>	<b>89.53</b>	98.84	2.81	<b>100</b>	<b>100</b>	<b>100</b>	<b>0</b>

TABLE II: Localization results on 20 images of size  $256 \times 256$ . In the pixel-wise metrics, everything is computed pixel by pixel. In the block-wise metrics, each  $8 \times 8$  block belongs to the positive class if at least one pixel of this block belongs to this class. This rule applies to prediction and the ground truth.

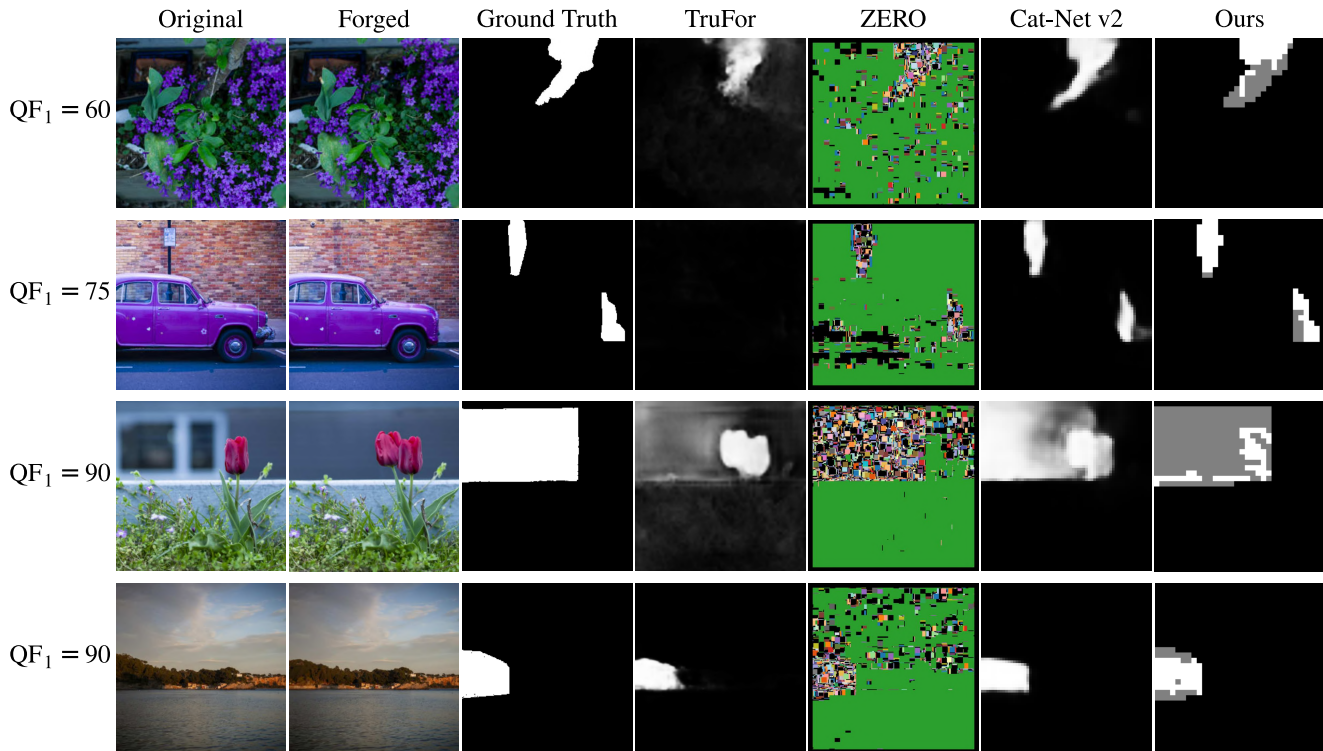


Fig. 8: Visual comparison of inpainting localization. Forged images are in bitmap format (PNG) but were compressed using  $QF_1$  60, 75, 90, and 90 from top to bottom. In the predictions of our method, white corresponds to incompatible blocks, gray corresponds to unsolved blocks and black is for compatible blocks after  $N = 100$  iterations.

prediction. This is done to evaluate how well models can distinguish each region. Let TP, FP, TN, and FN be the number of True Positive, False Positive, True Negative, and False Negative respectively. The True Positive Rate (TPR) is defined as  $TPR = TP/(TP + FN)$  and the True Negative Rate (TNR) is defined as  $TNR = TN/(FP + TN)$ . We will be using the balanced accuracy defined as:

$$ACC = \frac{TPR + TNR}{2}, \quad (16)$$

the  $F_1$  score is defined as:

$$F_1 = \frac{2TP}{2TP + FP + FN}, \quad (17)$$

the False Positive Rate is defined as:

$$FPR = \frac{FP}{FP + TN} \quad (18)$$

and the Area Under the Curve (AUC).

## B. Results

For the single compression setup, Fig. 8 shows a visualization of the output of our method compared to other forgery localization methods, and Table II shows the metrics associated with this experiment. We can see that all models are relatively good for this task but our method is slightly better in terms of false positives especially if we use block-wise metrics. These results match the statistics obtained in the

last section: all compatible blocks are detected as is and some incompatible blocks are also found. The gray blocks in our prediction represent unsolved blocks. Those are clipped blocks for which the theoretical upper bound can not be applied so the searching space is not reduced and the algorithm is not able to explore all the space.

For the double compression setup, the visual results are presented in Fig. 9. As expected, when  $QF_1$  is bigger than  $QF_2$ , all blocks are compatible and we are not able to detect any forgery. However, in the other case, when  $QF_1$  is smaller than  $QF_2$ , the detection is very good compared to the state-of-the-art methods. Note that when  $QF_1 = QF_2 > 85$  we are also able to detect parts of the forgery. Moreover, in a double compression setup, we can see that blocks are either compatible or unsolved and there are no incompatible blocks. This is because the upper bound is not tight enough and is not able to reduce the searching space enough to bring it to a reasonable size that could be entirely explored.

Table III and Table IV show the pixel-wise and block-wise metrics associated with this experiment. Again the metrics of our method match very closely to the statistics of the last section. In particular, Table IV clearly shows no FPR when we use the block-wise metrics (computed over more than 1M predictions). There is also no detection when  $QF_1$  is bigger than  $QF_2$  which was expected based on the last section statistics but note that, other state-of-the-art methods also have poor results in this setup. When  $QF_1$  is smaller than  $QF_2$ ,

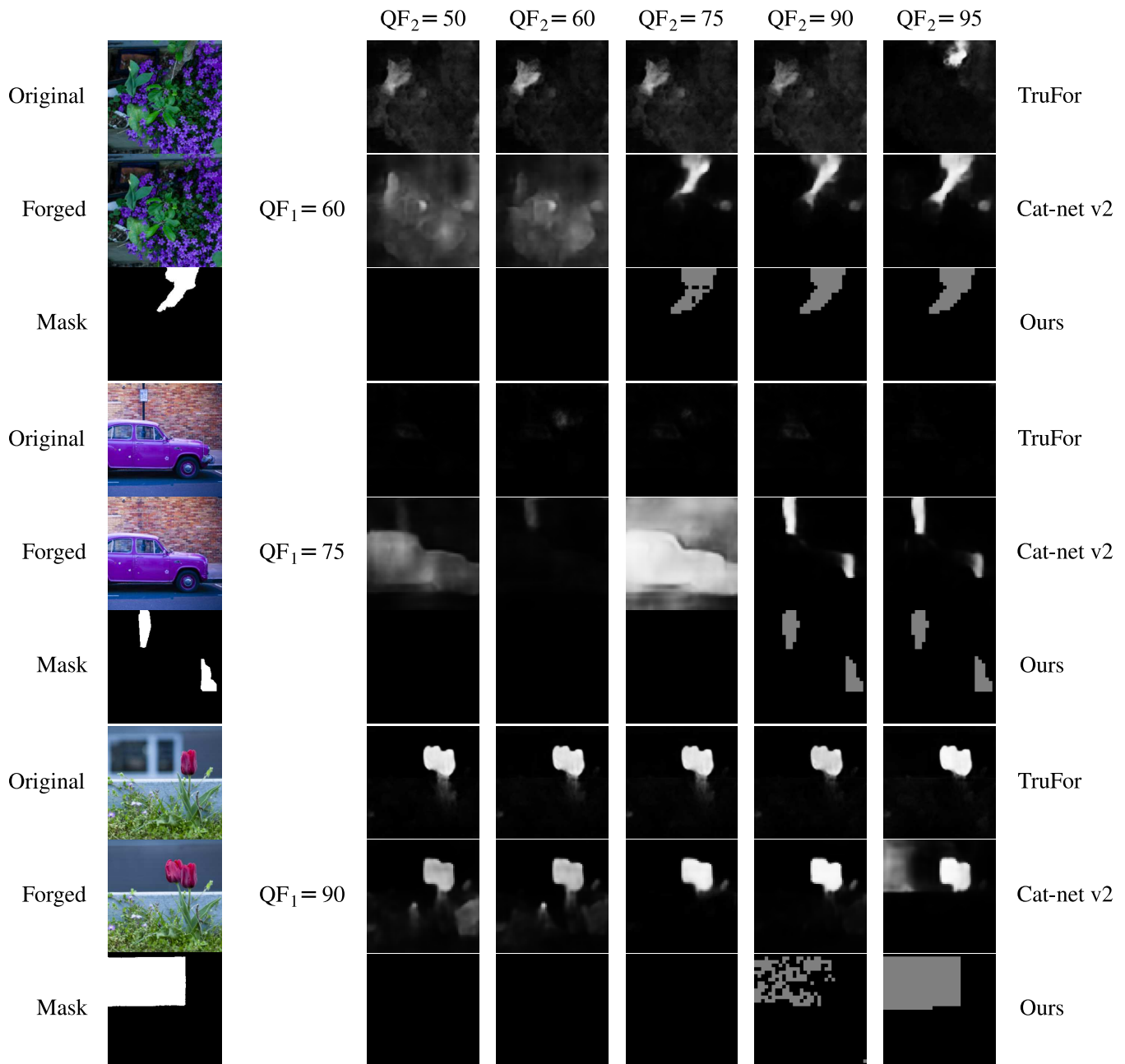


Fig. 9: Localization results in double-compressed inpainted images. Each image has been compressed at  $QF_1$ , modified in the pixel domain, and recompressed at  $QF_2$ . The detection is done on the DCT coefficients  $\mathbf{E}$  for all models. In our predictions, gray corresponds to unsolved blocks, and black to compatible blocks with  $N = 5000$  iterations. There are no incompatible blocks because theoretical constraints in double compression are not tight enough to efficiently reduce the search space.

our method outperforms other methods with close-to-perfect detection.

## VII. CONCLUSION AND PERSPECTIVES

### A. Conclusion

This paper has presented a new approach to solving the problem of verifying the authenticity of an image under the assumption that they were JPEG compressed before a potential forgery. Our method is based on the notion of compatibility of JPEG blocks (existence of an antecedent) or incompatibility

(absence of antecedent) which makes it very reliable under some assumptions (no False Positive). We extended this notion of compatibility to any number of compression, decompression or color transforms. We proposed a local search algorithm to look after the antecedent and combined it with a theoretical upper bound to reduce the search space.

We have seen that the type of modification (inpainting, splicing, or copy-move) can create up to 3 types of mismatch (grid, quantization table, and pipeline mismatch). We then studied the link between mismatch type and block compat-

		60					75					90				
		50	60	75	90	95	50	60	75	90	95	50	60	75	90	95
TruFor	ACC	<b>56.46</b>	52.81	60.05	68.89	75.71	<b>64.34</b>	57.53	<b>57.88</b>	63.07	75.39	50.99	51.05	50.82	51.65	57.97
	$F_1$	<b>17.16</b>	13.46	24.49	42.39	56.54	<b>31.98</b>	16.7	<b>19.01</b>	32.03	54.21	4.27	4.51	3.61	6.5	23.6
	AUC	<b>77.41</b>	76.25	75.59	80.03	89.98	<b>74.46</b>	71.66	<b>68.82</b>	82.13	86.25	70.91	68.73	69.24	68.9	71.03
	FPR	<b>0.02</b>	2.78	1.45	8.04	7.9	<b>0.87</b>	<b>0.78</b>	<b>0.63</b>	1.59	2.11	0.51	0.52	0.5	0.5	0.62
Cat-Net v2	ACC	53.66	<b>56.02</b>	68.25	70.14	70.95	58.54	<b>64.66</b>	53.11	83.66	78.94	54.94	54.45	52.79	52.55	66.55
	$F_1$	12.94	<b>13.63</b>	41.5	48.2	48.59	20.63	<b>33.81</b>	20.13	74.61	63.88	18.5	17.22	9.72	22.5	40.0
	AUC	71.77	<b>69.33</b>	87.84	97.7	98.65	71.26	<b>79.72</b>	66.06	98.1	97.61	73.31	70.15	70.68	65.91	97.81
	FPR	8.83	<b>6.14</b>	<b>0.66</b>	<b>0.2</b>	<b>0.24</b>	2.17	1.85	11.75	<b>0.81</b>	<b>0.88</b>	4.21	7.28	1.94	15.21	<b>0.54</b>
Ours	ACC	50	50	<b>96.23</b>	<b>98.58</b>	<b>98.57</b>	50	50	50	<b>98.76</b>	<b>98.73</b>	50	50	50	<b>58.78</b>	<b>98.58</b>
	$F_1$	0	0	<b>88.3</b>	<b>89.89</b>	<b>89.47</b>	0	0	0	<b>88.91</b>	<b>88.47</b>	0	0	0	<b>27.34</b>	<b>91.73</b>
	AUC	50	50	<b>96.23</b>	<b>98.58</b>	<b>98.57</b>	50	50	50	<b>98.76</b>	<b>98.73</b>	50	50	50	<b>58.78</b>	<b>98.58</b>
	FPR	0	0	2.37	2.65	2.81	0	0	0	2.39	2.52	0	0	0	<b>0.25</b>	2.83

TABLE III: Localization results on 100 images of size  $256 \times 256$  using pixel-wise metrics. Gray numbers are used for inaccurate methods with balanced accuracy below 55%. Bold numbers represent the best value in each category.

		60					75					90				
		50	60	75	90	95	50	60	75	90	95	50	60	75	90	95
TruFor	ACC	<b>57.57</b>	53.74	61.57	71.4	77.37	<b>65.37</b>	58.01	<b>58.56</b>	65.42	77.48	51.29	51.95	51.07	52.15	58.5
	$F_1$	<b>20.12</b>	16.87	28.39	46.12	60.7	<b>34.49</b>	18.15	<b>21.05</b>	37.06	58.15	5.49	7.66	4.63	9.22	26.33
	AUC	<b>78.15</b>	76.77	75.76	78.86	88.68	<b>73.8</b>	70.98	<b>68.23</b>	81.5	85.17	71.29	68.85	69.91	69.14	70.89
	FPR	<b>0</b>	3.64	3.05	8.62	8.24	<b>1.02</b>	<b>0.82</b>	<b>0.57</b>	1.63	2.62	0.67	0.79	0.67	0.91	1.46
Cat-Net v2	ACC	53.56	<b>56.04</b>	68.87	71.83	72.79	60.07	<b>65.98</b>	54.4	85.48	81.0	<b>55.69</b>	<b>55.15</b>	53.05	52.39	67.4
	$F_1$	15.47	<b>15.54</b>	43.3	51.82	52.59	24.88	<b>36.14</b>	24.25	77.89	68.63	<b>21.91</b>	<b>20.66</b>	10.77	23.99	43.12
	AUC	72.58	<b>69.99</b>	87.32	97.09	98.09	72.3	<b>80.09</b>	67.12	97.63	97.04	<b>71.8</b>	<b>68.62</b>	69.42	65.13	97.88
	FPR	9.85	<b>6.72</b>	0.77	0.22	0.25	2.59	1.62	12.44	1.03	1.0	<b>5.73</b>	<b>9.06</b>	2.83	16.36	0.71
Ours	ACC	50	50	<b>96.0</b>	<b>98.99</b>	<b>99.53</b>	50	50	50	<b>99.33</b>	<b>99.85</b>	50	50	50	<b>58.26</b>	<b>99.77</b>
	$F_1$	0	0	<b>95.78</b>	<b>98.97</b>	<b>99.52</b>	0	0	0	<b>99.32</b>	<b>99.85</b>	0	0	0	<b>25.89</b>	<b>99.77</b>
	AUC	50	50	<b>96.0</b>	<b>98.99</b>	<b>99.53</b>	50	50	50	<b>99.33</b>	<b>99.85</b>	50	50	50	<b>58.26</b>	<b>99.77</b>
	FPR	0	0	<b>0</b>	<b>0</b>	<b>0</b>	0	0	0	<b>0</b>	<b>0</b>	0	0	0	<b>0</b>	<b>0</b>

TABLE IV: Localization results on 100 images of size  $256 \times 256$  using block-wise metrics. Gray numbers are used for inaccurate methods with balanced accuracy below 55%. Bold numbers represent the best value in each category.

ibility. In particular, we saw that when we look at the pixel image without recompression, almost all mismatched blocks will be incompatible and easy to detect. But when looking at the recompressed (or recompressed then decompressed) image, some modified blocks may remain compatible because of the quantization tables used.

Finally, we conducted a forgery localization experiment to compare with state-of-the-art methods. It appears that without recompression, our method can accurately detect every modified block without error and thus outperforms other methods. If the image is recompressed after modification, our method can be very accurate when the second compression is weaker than the first one and also outperforms other methods. However, if the second compression is stronger than the first one, our method is unable to detect anything.

## B. Perspectives

This work should be seen as a proof of concept of using JPEG compatibility to detect modified images. Indeed, this method requires strong assumptions to work properly. In particular, the exact JPEG pipeline of the original image must be known up to its DCT algorithm implementation. For future work, there are at least two axes to transform this method into an off-the-shelf model.

The first axis is to make it more robust to unknowns. We could start to generalize it to unknown quantization tables by estimating a dictionary of potential tables and verifying the compatibility using each table. But the real challenge is to make it robust to any DCT (and IDCT) algorithm to be able to handle any image without knowing its main pipeline. The second axis is to improve the speed of the algorithm. For high  $QF$ , the algorithm requires thousands of iterations for a single block to ensure no False Positive. This means that for big images, it can take hours to analyze them. The speed could be improved either by finding tighter upper bounds to reduce the search space or by finding a new algorithm to find antecedent (or prove incompatibility). In particular, we believe the upper bound could be improved with a probabilistic constraint on the neighborhood. This would create a trade-off between a controlled False Positive Rate and the algorithm efficiency.

Finally, this method only relies on the property of non-surjectivity of compression and decompression processes. Such property could exist in other compressed formats. For example, forgery H26x or HEIC formats could be the source of incompatibilities.

## ACKNOWLEDGMENTS

The work presented in this paper received funding from the European Union's Horizon 2020 research and innovation

program under grant agreement No 101021687 (project “UNCOVER”). We also thank Antoine Mariot for helping us by forging images.

## REFERENCES

- [1] Yukihiro Arai, Takeshi Agui, and Masayuki Nakajima. A fast dct-sq scheme for images. *IEICE TRANSACTIONS (1976-1990)*, 71(11):1095–1097, 1988.
- [2] M. Barni, L. Bondi, N. Bonettini, P. Bestagini, A. Costanzo, M. Maggini, B. Tondi, and S. Tubaro. Aligned and non-aligned double JPEG detection using convolutional neural networks. 49:153–163, 2017.
- [3] Tiziano Bianchi and Alessandro Piva. Detection of nonaligned double jpeg compression based on integer periodicity maps. *IEEE transactions on Information Forensics and Security*, 7(2):842–848, 2011.
- [4] Jan Butora and Jessica Fridrich. Reverse jpeg compatibility attack. *IEEE Transactions on Information Forensics and Security*, 15:1444–1454, 2019.
- [5] Davide Cozzolino and Luisa Verdoliva. Noiseprint: A CNN-Based Camera Model Fingerprint. 15:144–159, 2020.
- [6] Eli Dworkatzky, Edgar Kaziakhmedov, and Jessica Fridrich. Advancing the jpeg compatibility attack: Theory, performance, robustness, and practice. In *Proceedings of the 2023 ACM Workshop on Information Hiding and Multimedia Security*, pages 67–79, 2023.
- [7] Hany Farid. Exposing digital forgeries from JPEG ghosts. 4(1):154–160, 2009.
- [8] Jessica Fridrich, Miroslav Goljan, and Rui Du. Steganalysis based on JPEG compatibility. In *Multimedia Systems and Applications IV*, volume 4518, pages 275–280. SPIE, 2001.
- [9] Dongdong Fu, Yun Q Shi, and Wei Su. A generalized benford’s law for jpeg coefficients and its applications in image forensics. In *Security, Steganography, and Watermarking of Multimedia Contents IX*, volume 6505, pages 574–584. SPIE, 2007.
- [10] Fabrizio Guillaro, Davide Cozzolino, Avneesh Sud, Nicholas Dufour, and Luisa Verdoliva. Trufor: Leveraging all-round clues for trustworthy image forgery detection and localization. In *Proceedings of the IEEE/CVF Conference on Computer Vision and Pattern Recognition*, pages 20606–20615, 2023.
- [11] IJG. libjpeg. <https://libjpeg.sourceforge.net/>, 1990.
- [12] Myung-Joon Kwon, Seung-Hun Nam, In-Jae Yu, Heung-Kyu Lee, and Changick Kim. Learning JPEG Compression Artifacts for Image Manipulation Detection and Localization. 130(8):1875–1895, 2022.
- [13] Etienne Levecque, Jan Butora, and Patrick Bas. Finding Incompatibles Blocks for Reliable JPEG Steganalysis. preprint on arxiv at <http://arxiv.org/abs/2402.13660>, 2024.
- [14] Andrew B. Lewis and Markus G. Kuhn. Exact JPEG recompression. In *Visual Information Processing and Communication*, volume 7543, pages 256–264. SPIE, 2010.
- [15] Christoph Loeffler, Adriaan Ligtenberg, and George S Moschytz. Practical fast 1-d dct algorithms with 11 multiplications. In *International Conference on Acoustics, Speech, and Signal Processing.*, pages 988–991. IEEE, 1989.
- [16] Jan Lukáš and Jessica Fridrich. Estimation of Primary Quantization Matrix in Double Compressed JPEG Images. 2003.
- [17] Tina Nikoukhah, Jérémy Anger, Miguel Colom, Jean-Michel Morel, and Rafael Grompone von Gioi. Zero: a local jpeg grid origin detector based on the number of dct zeros and its applications in image forensics. *Image Processing On Line*, 11:396–433, 2021.
- [18] Cecilia Pasquini, Giulia Boato, and Fernando Pérez-González. Multiple jpeg compression detection by means of benford-fourier coefficients. In *2014 IEEE International Workshop on Information Forensics and Security (WIFS)*, pages 113–118. IEEE, 2014.
- [19] Ali Taimori, Farbod Razzazi, Alireza Behrad, Ali Ahmadi, and Masoud Babaie-Zadeh. Quantization-Unaware Double JPEG Compression Detection. 54(3):269–286, 2016.
- [20] Yue Wu, Wael AbdAlmageed, and Premkumar Natarajan. ManTra-Net: Manipulation Tracing Network for Detection and Localization of Image Forgeries With Anomalous Features. pages 9543–9552, 2019.
- [21] Fabian Zach, Christian Riess, and Elli Angelopoulou. Automated image forgery detection through classification of JPEG ghosts. In *Joint DAGM (German Association for Pattern Recognition) and OAGM Symposium*, pages 185–194. Springer, 2012.